Research Article | Vol. 27, No. 3 | 4 Feb 2019 | OPTICS EXPRESS 3409
Optics EXPRESS

Resonance/non-resonance doublet-based self-absorption-free LIBS for quantitative analysis with a wide measurement range

J. J. HOU,[1,2] L. ZHANG,[1,2,*] Y. ZHAO,[1,2] W. G. MA,[1,2] L. DONG,[1,2] W. B. YIN,[1,2,*] L. T. XIAO,[1,2] AND S. T. JIA[1,2]

[1]*State Key Laboratory of Quantum Optics and Quantum Optics Devices, Institute of Laser Spectroscopy, Shanxi University, Taiyuan 030006, China*
[2]*Collaborative Innovation Center of Extreme Optics, Shanxi University, Taiyuan 030006, China*
**k1226@sxu.eud.cn*

Abstract: A resonance/non-resonance, doublet-based, self-absorption-free, laser-induced breakdown spectroscopy (SAF-LIBS) technique is proposed for greatly expanding the measurement range of quantitative elemental analysis by using a quasi-optically thin line. The quasi-optically thin spectral line is obtained by matching the measured doublet atomic lines' intensity ratios with the theoretical one, and the applicable measurement range is expanded by utilizing the resonance and non-resonance lines. The specific calibration process consists of two parts: the nonlinear LIBS calibration and the linear SAF-LIBS calibration. For quantitative measurements, the approximate content of the unknown sample is determined first by using the LIBS calibration curve, and then the SAF-LIBS spectra and the resonance or non-resonance calibration curve that corresponds to the predetermined content are used for further implementing the quantitative analysis. Univariate quantitative analysis results of Cu show that this resonance/non-resonance doublet-based SAF-LIBS technique not only captures the quasi-optically thin spectral line in a wide range of elemental content, but also possesses high correlation coefficients of calibration curves, small relative errors of measurement and low limits of detection. The applicability and limitations of this technique are also discussed, and the evolution as well as the related major determinants of self-absorption are analyzed by taking advantage of the spatial-temporal evolution images of plasma emissivity.

1. Introduction

Laser-induced breakdown spectroscopy (LIBS) is a spectrochemical analysis technique based on emission spectroscopy. In recent years, it has shown great potential in fields of industrial process control, environmental monitoring, biomedical research, etc. due to its advantages such as real-time, in situ, simultaneous multi-element analysis and no sample preparation [1–10]. In order to make this technique mature, many researchers have proposed different solutions to various problems encountered in the application of LIBS to improve its analytical performance. Actually, the spontaneous emissions of laser-induced plasma are subject to absorption when they travel from the interior of plasma to the outside because there are in its path atoms or molecules of the same kind that cause the emission. This phenomenon is the so-called self-absorption effect, which not only weakens the spectral line intensity and increases its full width at half maximum (FWHM) [11,12], but also causes saturation effects in univariate calibration. The self-absorption is an inevitable process in the interaction of electromagnetic waves and plasma. There presented a lot of work on the mechanism of self-absorption, which were devoted to weakening its undesired effects and improving the measurement accuracy. Some commonly used methods include the self-absorption (*SA*) coefficient correction, plasma modeling, internal standard reference, laser or microwave assisted LIBS, etc. For example, Sherbini *et al.* [13] proposed a method for correcting the

#349350 https://doi.org/10.1364/OE.27.003409
Journal © 2019 Received 29 Oct 2018; revised 30 Dec 2018; accepted 18 Jan 2019; published 31 Jan 2019

Optics EXPRESS

self-absorption effect by calculating *SA* coefficients of emission lines from the spectral line width, and verified that the self-absorption correction can avoid the systematic error of the electron temperature caused by the uncorrected values of the line intensity. Gornushkin *et al.* [14] established a theoretical model for optically thick and inhomogeneous plasmas to determine the degrees of self-absorption of emission lines by considering the reabsorption process, the continuum radiation and the absorption coefficient. Sun *et al.* [15] employed an internal reference to make correction of the self-absorption effect in CF-LIBS, and found that the linearity of all points on the Boltzmann plot was enhanced and the accuracy of the quantitative analysis results was improved. But all these methods tend to be complex and time consuming, and require some fulfilled conditions and additional plasma parameters. Also some approximations and assumptions made in these calculation methods may lead to deviation between the quantitative results and real values. The laser-stimulated absorption assisted LIBS and microwave-assisted excitation LIBS techniques proposed by Guo *et al.* [16,17] provide other approaches for eliminating the self-absorption effect. Although as a result, the number density of the ground-state atoms that related to the degree of self-absorption decreased sharply, these techniques require continuous wavelength tunable laser or continuous microwave generator to re-excite the plasma, which greatly limits their applications due to the large size and high cost. We recently proposed a self-absorption-free LIBS (SAF-LIBS) technique [18,19] to directly capture quasi-optically thin spectral line by matching the measured doublet atomic lines intensity ratios with the theoretical one. By evaluating the *SA* coefficient and Boltzmann plot linearity, it was confirmed that this technique is qualified to collect quasi-optically thin plasma spectrum nearby a certain wavelength and realize accurate chemical composition measurements. However, the applicability analysis results of SAF-LIBS demonstrated a relatively narrow applicable measurement range (e.g. 0-15.9% for Al), which severely limits its further widespread application. Therefore, how to greatly expand the applicable measurement range of SAF-LIBS becomes an urgent challenge.

In general, the ground state population is larger than the excited one in a plasma, and the resonance transition connects a low-lying excited level to the ground state of the atom, while the low level of non-resonance transition is a highly excited state. Although the resonance line is susceptible to self-absorption, it has higher sensitivity. Conversely, the non-resonance line is less subject to self-absorption but has poor sensitivity [20]. It has been noticed that the resonance line is suitable for the detection of trace elements, while the non-resonance line is suitable for the detection of major elements due to its calibration curve has a wider measurement range. Therefore, we wonder if the resonance and non-resonance doublets could be introduced into SAF-LIBS to greatly expand the applicable measurement range while maintaining the detection sensitivity.

To validate the above ideas and enhance the applicability of SAF-LIBS, a resonance/non-resonance doublet based SAF-LIBS technique was proposed in this paper. It is worth noting that due to the limitation of the resolution of our spectrometer, we chose Cu instead of Al to demonstrate the feasibility. By combining the resonance Cu I 325 nm and non-resonance Cu I 520 nm doublets with SAF-LIBS, the univariate linear calibration curve of Cu will be established according to the quasi-optically thin requirements. Then according to the quantitative results by resonance/non-resonance doublet based SAF-LIBS, we will give a discussion on its performance including applicable measurement range, measurement accuracy, limit of detection (LOD), etc.

2. Experimental and methodology

2.1 Experimental

The details of the entire experimental LIBS system have described previously [18,19] and will only be summarized here. A Q-Switched Nd: YAG laser (Spectra Physics, INDI-HG-20S) operating at the fundamental wavelength of 1064 nm was employed as the ablation

Optics EXPRESS

source, with a pulse duration of 7 ns, a repetition rate of 20 Hz, and a fixed energy of 50 mJ/pulse. The laser beam was focused at the sample surface by an objective lens with a focal length of 75 mm, and the diameter of the focal spot was approximately 600 μm. A condenser lens with a focal length of 75 mm was aligned with the laser-produced plasma to generate a 4 × magnified image of the plume. Then the image along the line of sight perpendicular to the laser beam was delivered to a grating spectrograph (Princeton Instruments, SP-2750) that equipped with a time gated ICCD (Princeton Instruments, PI-MAX4-1024i) by a 200 μm optical fiber. Another ICCD (Andor, iStar DH334T) was used as a camera to record the emissivity images of plasma via dual-wavelength differential imaging [21,22]. In our experiment, the integration time for spectra acquisition was 100 ns and the delay time was in the range of 200-800 ns with identical interval of 100 ns.

The samples used in the experiment were twelve pressed tablets of finely powdered potassium bromide and copper oxide, with the copper content covering a range of 0.01-60 *wt*%.

2.2 Methodology

Assuming the plasma is homogeneous and in a local thermodynamic equilibrium (LTE) condition during spectra acquisition, the theoretical doublet intensity ratio of an element in ionization stage Z can be expressed as [23]:

$$\frac{I_1}{I_2} = \left(\frac{\lambda_{nm,Z}}{\lambda_{ki,Z}}\right)\left(\frac{A_{ki,Z}}{A_{nm,Z}}\right)\left(\frac{g_{k,Z}}{g_{n,Z}}\right)\exp\left(-\frac{E_{k,Z}-E_{n,Z}}{k_B T}\right), \quad (1)$$

where I_1 is the line intensity from the k-i transition and I_2 is that from the n-m transition, λ is the transition wavelength, A is the transition probability, g is the degeneracy, E is the upper level energy, k_B is the Boltzmann constant, and T is the plasma temperature. When the doublet lines have comparable upper levels, the temperature dependent exponential item in the equation can be ignored and this intensity ratio tends to be a constant that is independent of time and experimental conditions. By matching this ratio with the measured values at different delay times, one can find out the exact time interval (at a delay time with a certain integration time) where the spectral line is closest to optically thin condition and realize SAF-LIBS.

For an element with both resonance and non-resonance doublets, the quantitative measurement process of resonance/non-resonance doublet based SAF-LIBS can be briefly summarized as: firstly, establish the univariate calibration curve of non-resonance line by LIBS and the univariate multi-segment calibration curve of resonance and non-resonance lines by SAF-LIBS. Next, determine the content segment to which the unknown sample belongs by substituting the intensity of non-resonance line into the nonlinear LIBS calibration equation, and then perform further quantitative analysis by the corresponding segmented calibration curve.

3. Results and discussion

3.1 Realization of resonance/non-resonance doublet based SAF-LIBS

The typical average spectrum of the tablet samples is shown in Fig. 1 (delay time of 500 ns, integration time of 100 ns, tablet with 6% copper), which covers a spectral region from 300 to 550 nm. The selected copper lines as well as their detailed spectroscopic parameters are listed in Table 1, taken from the NIST atomic database. The doublet Cu I 324.75 nm and Cu I 327.40 nm ($3d^{10}4p$-$3d^{10}4s$) are resonance lines, while the doublet Cu I 515.32 nm and Cu I 521.82 nm ($3d^{10}4d$-$3d^{10}4p$) are non-resonance lines. Due to the close upper level energies of these two doubles, they were employed to determine the time intervals where the emission lines are quasi-optically thin and to perform quantitative analysis in the following

Optics EXPRESS

experiments. The non-resonance lines at 465.11 nm and 510.55 nm were also used for plasma temperature calculation.

Table 1. Spectroscopic parameters of the copper spectral lines.

Transition type	Wavelength (nm)	Transition Probability (sec^{-1})	Statistical Weight	Upper Level Energy (eV)	Lower Level Energy (eV)
Resonance	324.75	1.40×10^8	4	3.82	0.00
	327.40	1.38×10^8	2	3.79	0.00
Non-resonance	465.11	3.80×10^7	8	7.74	5.07
	510.55	2.00×10^6	4	3.82	1.39
	515.32	6.00×10^7	4	6.19	3.79
	521.82	7.50×10^7	6	6.19	3.82

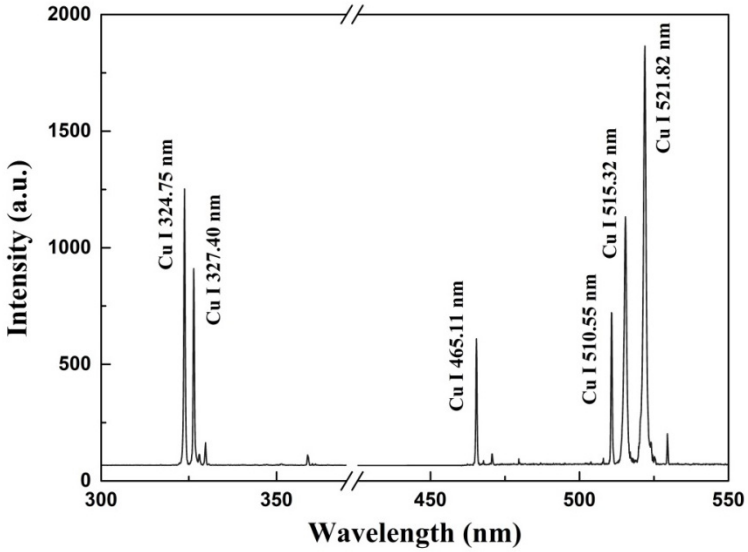

Fig. 1. Typical average spectrum of the tablets, in which both the resonance doublet around 325 nm and the non-resonance doublet around 520 nm are presented.

Combined these lines with Eq. (1), we studied the temporal evolution of intensity ratio of Cu resonance and non-resonance doublets. In order to obtain enough reproducibility of the emission spectra from plasma and compensate for sample inhomogeneity, 60 plasma spectra with background subtracted were averaged under identical experimental conditions. The results of the temporal evolution of the intensity ratio for resonance and non-resonance doublets and the optimal delay times are shown in the following.

3.1.1 SAF-LIBS for resonance doublet

Figures 2(a) and 2(b) give the temporal evolutions of the doublet intensity ratio of the resonance Cu I 324.75 nm and Cu I 327.40 nm lines in the time domain of 200 ns to 800 ns (note that the lifetime of exited Cu species was observed as ~800 ns) by using the tablets with Cu content in the ranges of 0.01% to 1% and 3% to 60%, respectively. The straight line represents the theoretical ratio value of 2.04. Figure 3 shows the relationship between the optimal delay time and the Cu content, where the time values for contents larger than 0.01% were predicted through linear fitting of the data points in Fig. 2 and expressed by hollow dot circles. It can be seen that the optimal delay time increased with the increase of Cu content, and the resonance lines could be considered as quasi-optically thin only for Cu content no larger than 0.01%. Thus, for resonance line, its quasi-optically thin emission can be captured only if the element content is relatively low. With the increase of element content, the self-

Optics EXPRESS

absorption effect became so serious that it was impossible to acquire any quasi-optically thin spectra. In addition, the temporal evolution curve of the 0.01% tablet in Fig. 2(a) indicates that the quasi-optically thin condition was reached twice at 245 ns and 782 ns during the plasma evolution. A similar trend was also found for the 0.05% tablet. The reasons for this will be discussed in detail in Section 3.2.

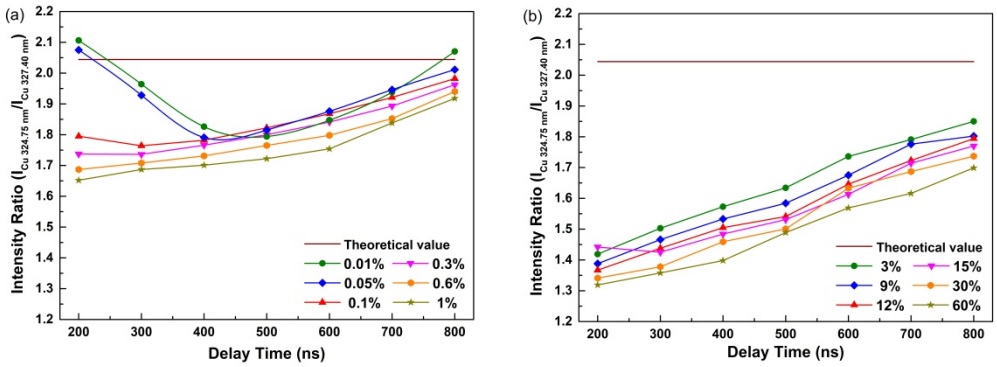

Fig. 2. Temporal evolution of intensity ratio of resonance doublet Cu I lines with content in the ranges of (a) 0.01-1% and (b) 3-60%.

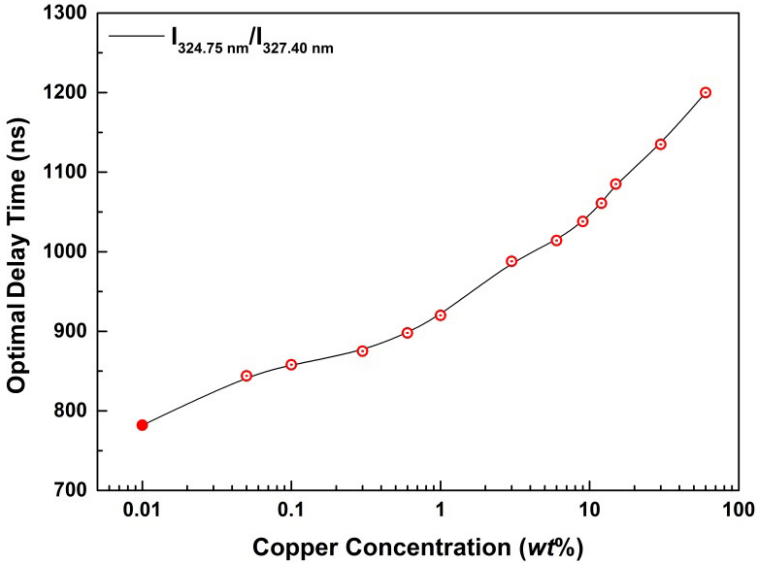

Fig. 3. Relationship between the optimal delay time of resonance Cu I doublet and the copper content.

3.1.2 SAF-LIBS for non-resonance doublet

Figures 4(a) and 4(b) show the temporal evolution of the doublet intensity ratio of the non-resonance Cu I 521.82 nm and Cu I 515.32 nm lines in the time domain of 200-800 ns by using the tablets with Cu content in the ranges of 0.01% to 1% and 3% to 60%, respectively. The straight line represents the theoretical ratio value of 1.85. Figure 5 shows the relationship between the optimal delay time and the Cu content, where the time for the content of 60% was predicted through linear fitting of the data points in Fig. 4(b) and is expressed by a hollow circle. It can be seen that the optimal delay time increased with the increase of Cu content, and the non-resonance lines could be considered as quasi-optically thin over a wide content range of 0.01-30%. However, when the content was larger than 60%, the quasi-

Optics EXPRESS

optically thin lines could never be captured during the lifetime of plasma. For tablets with Cu content in the ranges of 0.01-0.05%, 0.1-1%, and 3-30%, the corresponding acquisition delay times closest to the optimal delay times are defined as t_{ot}, which were determined to be 400 ns, 500 ns, and 600 ns respectively, and are circled by dotted ellipses in Fig. 4. Thus, for non-resonance line, its quasi-optically thin emission could be captured over a wide elemental content range.

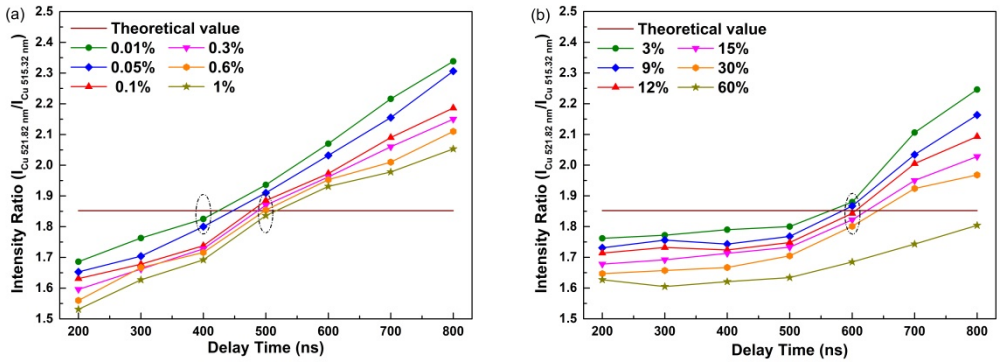

Fig. 4. Temporal evolution of intensity ratio of non-resonance Cu I doublet with content in the ranges of (a) 0.01-1% and (b) 3-60%.

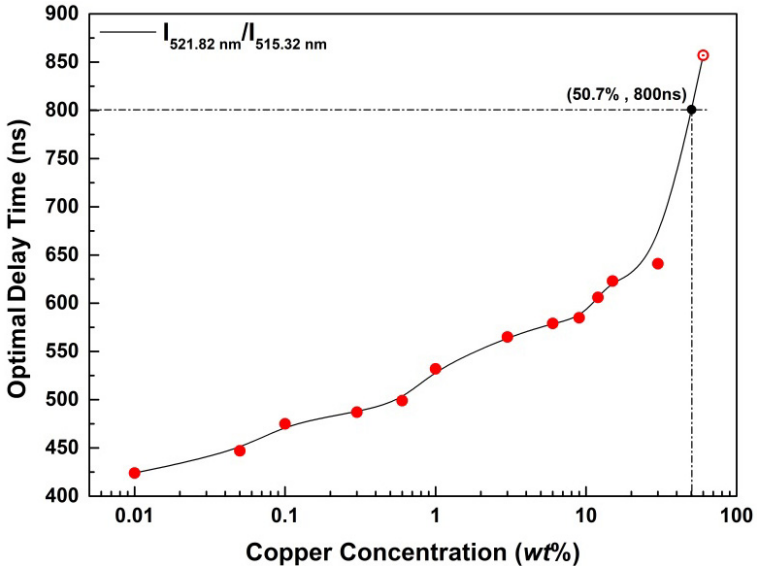

Fig. 5. Relationship between the optimal delay time of non-resonance Cu I doublet and the copper content.

3.2 Validation of self-absorption evolution

In section 3.1.1, an interesting experimental phenomenon was observed that during the plasma evolution, the resonance doublet emitted from low copper content tablet could reach the quasi-optically thin condition twice. The self-absorption effect occurred on the resonance doublet with higher copper content weakened with time, but could never be quasi-optically thin. In order to investigate the fundamental physical mechanism, the self-absorption effect of resonance Cu I 324.75 nm line existed in the plasmas of tablets with Cu content of 0.01%, 0.05% and 0.6% were investigated.

Optics EXPRESS

The *SA* coefficient indicates the self-absorption degree of a laser-produced plasma, and can be obtained by dividing the measured peak intensity by the expected one without self-absorption [13]:

$$SA = \frac{I(\lambda_0)}{I_0(\lambda_0)} = \frac{(1-e^{-\tau})}{\tau}, \tag{2}$$

where τ is the optical length (dimensionless) and when the Gaussian component of the line width is negligible with respect to the Lorentzian one,

$$\tau \approx K / \Delta\lambda_0 = 2\frac{e^2}{mc^2\Delta\lambda_0} n_i f \lambda_0^2 l, \tag{3}$$

where $\Delta\lambda_0$ is the expected FWHM of the emission line, e is the electron charge, m is the electron mass, c is the light speed, n_i is the energy number density of species in the i level, f is the transition oscillator strength, and l is the whole length of the absorption path over which the light travels. From Eqs. (2) and (3), it can be inferred that the *SA* decreases with the increase of K, which means that the larger the K, the more self-absorbed the emission line.

Combined with the Boltzmann distribution law and the relationship between oscillator strength and transition probability (Ladenburg formula), K can be expressed as [17]:

$$K = \frac{1}{4\pi^2 c}\frac{A_{ki} g_k}{Z(T)} e^{-\frac{E_i}{kT}} \lambda_0^4 \times Nl, \tag{4}$$

where $Z(T)$ is the partition function and N is the total number density of species in an atomic or ionic state. It shows that the self-absorption is proportional to the transition probability, degeneracy of upper level, wavelength, number density and length of the absorption path, and is inversely proportional to the lower energy level. Notice that the relationship between self-absorption and temperature varies with energy level.

In order to get the Nl for Cu in laser-induced plasma, the dual-wavelength differential imaging technique [21,22] was employed to measure the total number density and absorption path length of the Cu species. Sixty time-resolved plasma images with background subtracted were averaged to obtain good signal-to-noise ratio. Then the resulted emission images were further treated with the Abel inversion. The inversed images corresponded to the emissivity images of the studied species with respect to the chosen line, which can represent the total number density of atoms when the plasma is assumed to be in LTE state. Here, the line chosen for representing neutral Cu species was Cu I 521.82 nm but not Cu I 324.75 nm since they correspond to the same Nl, and the transmittance of the filter centered at 521 nm is much higher. These processed time-resolved emissivity images are shown in Fig. 6, where Figs. 6(a)-6(c) represent the tablets with Cu content of 0.01%, 0.05%, and 0.6%, respectively. The superscripts a to f in each figure indicate the delay times of 200, 300, 400, 600, 700 and 800 ns, respectively, and the horizontal white arrow line represents the line of sight. The integrals of emissivity that represent the Nl values are listed in Table 2. In addition, the electron temperatures were also calculated and shown in Table 2 by using the Boltzmann plot created from the five Cu I lines.

Optics EXPRESS

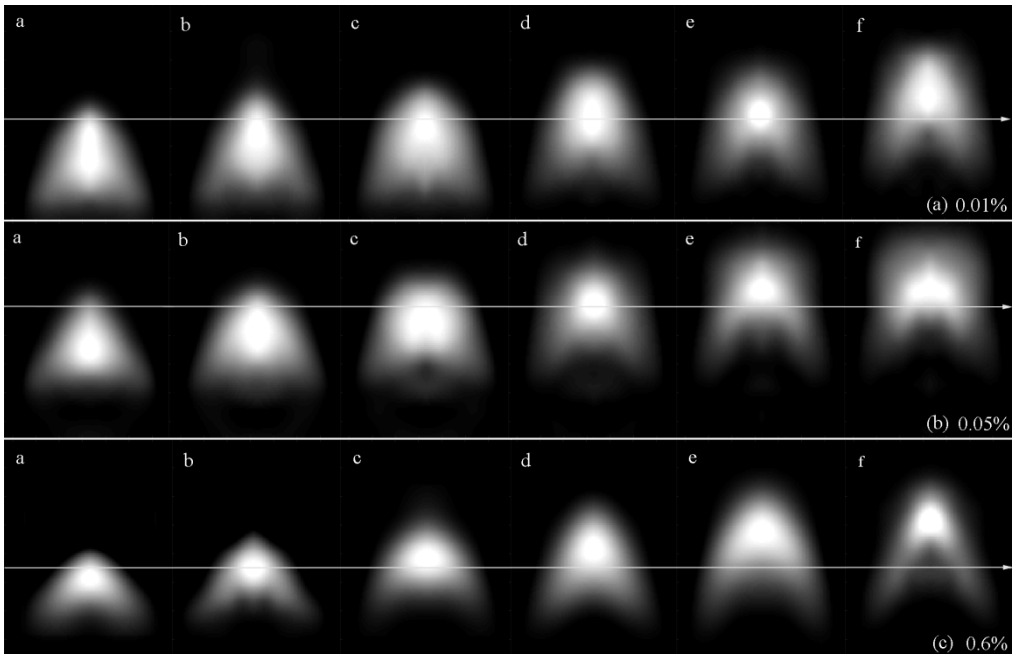

Fig. 6. Time-resolved emissivity images of the non-resonance Cu I 521.82 nm line for tablets with copper content of (a) 0.01%, (b) 0.05% and (c) 0.6%.

Table 2. The temporal parameters of SA coefficient of Cu I for tablets with various Cu contents.

Content (%)	Parameter	Time (ns)					
		200	300	400	600	700	800
0.01	*T* (K)	10890	10020	9188	8770	8610	8450
	Nl (a.u.)	3932	4500	5408	5700	4810	3200
0.05	*T* (K)	11032	10310	9316	8824	8705	8513
	Nl (a.u.)	3091	5178	6772	6212	5123	3869
0.60	*T* (K)	11103	10143	9843	9653	9363	9010
	Nl (a.u.)	6890	7160	6548	5615	4438	3026

According to Eq. (4) and the spectroscopic parameters of Cu 324.75 nm line listed in Tables 1 and 2, the *K* values of the three tablets against time are shown in Fig. 7. It can be seen that the *K* value for the 0.01% tablet increased initially and then decreased with time. Both in the early and late stages of plasma evolution, the self-absorption effects were weak due to the small volume and the fast expansion speed. It was consistent with the evolution curve of lines intensity ratio and implies that for a fixed observation position, the atomic number densities of the plasma in the ground state at some moments of evolution were really small and the self-absorption effect could be neglected reasonably. The *K* value for the 0.05% tablet increased rapidly and then decreased slowly over time indicates a weak self-absorption in the early stage of plasma evolution, while the *K* value for the 0.6% tablet increased slightly and then decreased rapidly indicates a weak self-absorption in the late stage of plasma evolution. These evolution curves of *K* had same trend as those of resonance lines intensity ratio.

Optics EXPRESS

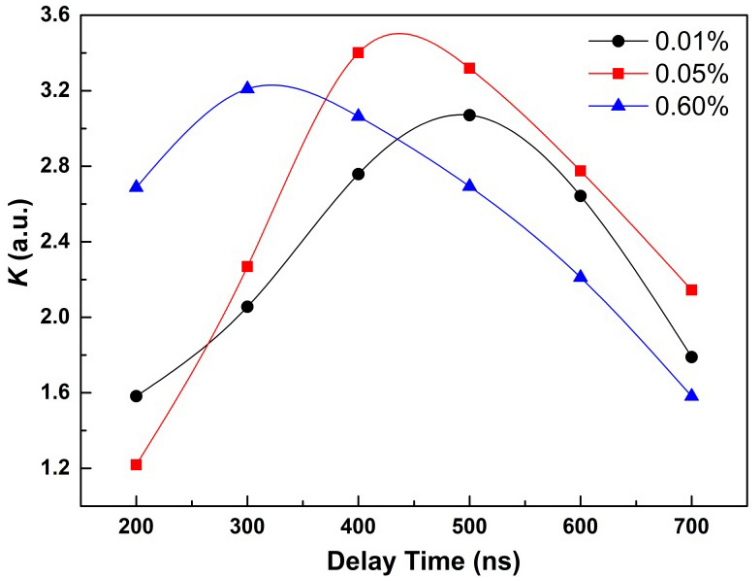

Fig. 7. Temporal evolution of K of resonance Cu I 324.75 nm line with Cu contents of 0.01%, 0.05% and 0.6%.

3.3 Calibration and performance test

Figure 8 shows the plots of relative error (RE) of measurement by using the resonance (Cu I 324.75 nm) and non-resonance (Cu I 521.82 nm) lines versus the Cu content at the acquisition delay time t_{ot}. The relative measurement errors were calculated by the equation: RE = 100* ((SA-LIBS measured value – nominal value)/nominal value). As can be seen, both the RE values of resonance and non-resonance lines decreased with the increase of Cu content. Because the two curves crossed at 0.48% (defined as C_{cross}), the resonance line was used for quantitative analysis when the copper content was below 0.48%, and the non-resonance line was used when the copper content was above 0.48%.

In order to verify the quantitative measurement accuracy and the measurement range of resonance/non-resonance doublet based SAF-LIBS, the univariate analysis of Cu was performed. The specific calibration and quantitative analysis process are as follows.

1) Calibration: firstly, establish the univariate LIBS calibration curve of non-resonance Cu I 521.82 nm line by using a series of standard samples, and then establish the univariate multi-segment calibration curve of resonance and non-resonance lines by SAF-LIBS according to the predetermined t_{ot}.

2) Quantitative analysis: determine the segment to which the unknown sample belongs by substituting the intensity of non-resonance line into the nonlinear LIBS calibration equation, and then perform further quantitative analysis by the corresponding segmented calibration curve.

Optics EXPRESS

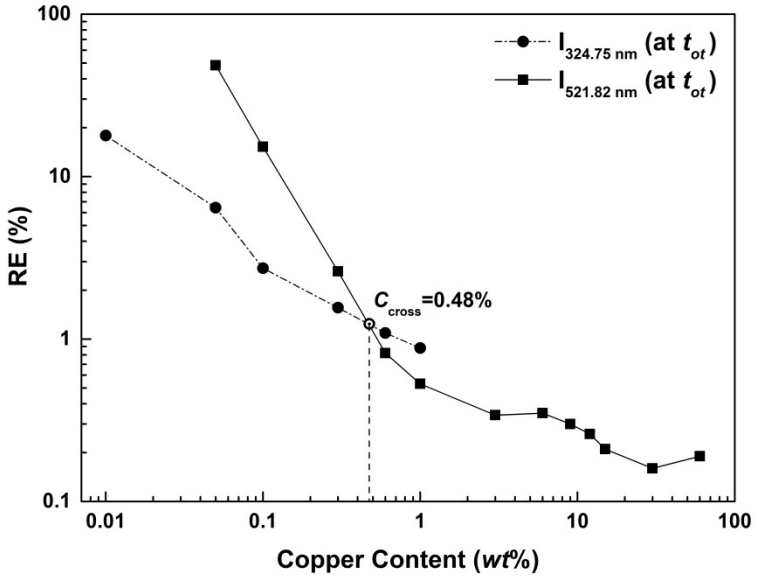

Fig. 8. Relationship between the RE of measurement by using the resonance Cu I 324.75 nm and non-resonance Cu I 521.82 nm lines and the Cu content.

Figure 9 shows the multi-segment calibration curve of Cu in the content range of 0-50.7% by SAF-LIBS and the quantitative analysis results for two unknown samples (marked as stars). The inset in the figure shows the magnified section of 0-1.0% Cu content. The multi-segment calibration curve can be divided into four segments, where segments S1 (0.01-0.1%) and S2 (0.1-0.48%) were created by the resonance line, and segments S3 (0.48-1.0%) and S4 (1.0-50.7%) were created by the non-resonance line. Each segment in the calibration curve corresponded to an individual acquisition delay time t_{ot}, and had a correlation coefficient R^2 greater than 0.99. The linear calibration equations for the four segments were y = 326.07x + 11.4, y = 61.7x + 38.3, y = 69.6x + 37.25, and y = 3x + 107, respectively. It can be seen that each segment in Fig. 9 exhibit a non-zero intercept. For low copper content (0.01%-1%) samples, the intercepts for segments S1, S2 and S3 on the x-axis are –0.035%, –0.62%, and –0.54%, respectively. In this case, the spectral lines at the optimal delay times could be considered as quasi-optically thin lines. However, for samples with copper contents larger than 1%, the intercept for segment S4 on the x-axis is –35.67%. In this case, the spectral lines at the optimal delay times were only the ones with the weakest self-absorption during plasma evolution, and they could be considered as weakest self-absorbed lines. The three breakpoints between the adjacent segments were caused by the differences in optically thinness of segments S1 and S2, spectral lines used in segments S2 and S3, and delay times t_{ot} used in segments S3 and S4.

Two tablets with copper content of 0.25% and 10% were used as unknown samples in the experiment for performance test purpose. After determining the segment of each sample by the LIBS, the copper contents of the two samples were quantitatively analyzed by using the calibration curves of segments S2 (resonance line) and S4 (non-resonance line), respectively. By substituting the line intensities of resonance Cu I 521.82 nm into the corresponding linear calibration equations, the copper contents in the two tablets were calculated to be 0.24% and 9.9%, respectively, corresponding to RE values of 4% and 1% (Fig. 9). The quantitative analysis results indicate that the resonance/non-resonance doublet based SAF-LIBS has high accuracy in a wide applicable measurement range.

Optics EXPRESS

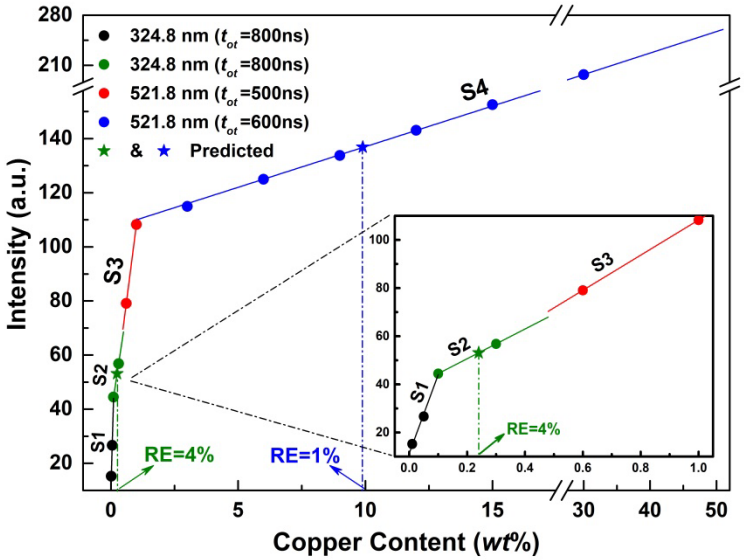

Fig. 9. Multi-segment calibration curve of Cu established by resonance/non-resonance doublet based SAF-LIBS over a wide content range of 0-50.7%.

In order to evaluate the detection sensitivity of resonance/non-resonance doublet based SAF-LIBS, the LOD was also estimated as 3 times the content to the signal-to-noise ratio of a relatively low content sample. In our experiment, the LOD was determined to be 1.35×10^{-4} *wt*% (1.35 ppm) based on the response to the 0.01% Cu tablet. Thus, introducing the resonance and non-resonance doublets into SAF-LIBS not only expands the applicable measurement range, but also maintains high sensitivity.

3.4 Applicability and limitations

The resonance/non-resonance doublet based SAF-LIBS is able to obtain quasi-optically thin spectral lines and perform high-precision quantitative analysis in a wide range of element content, but also has specific application and limitations. As shown in Fig. 5, the optimal delay time increased with the increase of element content, and the lifetime of the spectral line at the fixed observation line of sight was observed as 800 ns in our experiment. The Cu content corresponding to this lifetime point is estimated to be 50.7%, which is the limit of the applicable content for this technique. If the copper content exceeds this maximum limit, the quasi-optically thin spectral lines could never be captured during the plasma evolution. Therefore, considering the estimated LOD value, the applicable measurement range of resonance/non-resonance doublet based SAF-LIBS for copper is 1.35×10^{-4}-50.7%.

The limitations of resonance/non-resonance doublet based SAF-LIBS lie in three aspects. Firstly, it involves two basic assumptions, that is, the plasma is homogeneous and in the LTE state, which are considered to be satisfied in usual LIBS experiments. Secondly, it requires that the element to be analyzed should have both resonance and non-resonance doublets in the detection spectral range. Thirdly, the uncertainties of transition probability of spectral lines can introduce extra errors for estimating the optimal delay times, thus spectral lines with less uncertainty of transition probability are preferred.

4. Conclusions

In this work, resonance and non-resonance doublets were introduced into SAF-LIBS to expand its applicable elemental content range and enhance the quantitative performance. The nonlinear LIBS calibration and the linear multi-segment SAF-LIBS calibration were established for the univariate quantitative analysis of Cu, and the correlation coefficients R^2 of

Optics EXPRESS

all these curves were greater than 0.99. For quantitative measurements, to which segment the unknown sample belongs should be determined firstly by using the LIBS calibration curve. Then further quantitative analysis could be performed using the SAF-LIBS spectra and the resonance or non-resonance calibration curve that corresponds to the predetermined segment. The quasi-optically thin resonance line could be captured only when the element content was relatively low, while for non-resonance line, the quasi-optically thin line could be captured in a wide content range. Correspondingly, the evolution process of self-absorption as well as its related influencing factors was discussed by taking advantage of spatial-temporal emissivity imaging. Univariate quantitative analysis results showed that the RE values of tablets with copper content of 0.25% and 10% were 4% and 1%, respectively. The applicable measurement range for copper was estimated to be within 50.7%, while the LOD was of 1.35 ppm. This resonance/non-resonance doublet based SAF-LIBS technique can provide accurate chemical composition measurements over a wide elemental content range, and is expected to promote the practical processes of LIBS in industrial application.

Funding

National Key R&D Program of China (2017YFA0304203); Changjiang Scholars and Innovative Research Team in University of Ministry of Education of China (IRT_17R70); National Natural Science Foundation of China (NSFC) (61475093, 61875108, 61775125, 11434007); Major Special Science and Technology Projects in Shanxi (MD2016-01, 201804D131036); 111 project (D18001); Fund for Shanxi "1331KSC."

References

1. L. Torrisi, F. Caridi, and L. Giuffrida, "Comparison of Pd plasmas Produced at 532nm and 1064nm by a Nd:YAG laser ablation," Nucl. Instrum. Methods Phys. Res. B **268**(13), 2285–2291 (2010).
2. K. Aryal, H. Khatri, R. W. Collins, and S. Marsillac, "In situ and ex situ studies of molybdenum thin films deposited by RF and DC magnetron sputtering as a back contact for CIGS solar cells," Int. J. Photoenergy **2012**(1), 7863–7871 (2012).
3. Z. Wang, L. Z. Li, L. West, Z. Li, and W. D. Ni, "A spectrum standardization approach for laser-induced breakdown spectroscopy measurements," Spectrochim. Acta B At. Spectrosc. **68**(2), 58–64 (2012).
4. Z. Wang, T. B. Yuan, Z. Y. Hou, W. D. Zhou, J. D. Lu, H. B. Ding, and X. Y. Zeng, "Laser-induced breakdown spectroscopy in China," Front. Phys. **9**(4), 419–438 (2014).
5. Z. Wang, T. B. Yuan, S. L. Lui, Z. Y. Hou, X. W. Li, Z. Li, and W. D. Ni, "Major elements analysis in bituminous coals under different ambient gases by laser-induced breakdown spectroscopy with PLS modeling," Front. Phys. **7**(6), 708–713 (2012).
6. M. Gaft, E. Dvir, H. Modiano, and U. Schone, "Laser induced breakdown spectroscopy machine for online ash analyses in coal," Spectrochim. Acta B At. Spectrosc. **63**(10), 1177–1182 (2008).
7. S. C. Yao, J. D. Lu, K. Chen, S. H. Pan, J. Y. Li, and M. R. Dong, "Study of laser-induced breakdown spectroscopy to discriminate pearlitic/ferritic from martensitic phases," Appl. Surf. Sci. **257**(7), 3103–3110 (2011).
8. R. Hai, N. Farid, D. Y. Zhao, L. Zhang, J. H. Liu, H. B. Ding, J. Wu, and G. N. Luo, "Laser-induced breakdown spectroscopic characterization of impurity deposition on the first wall of a magnetic confined fusion device: experimental advanced superconducting tokamak," Spectrochim. Acta B At. Spectrosc. **87**(87), 147–152 (2013).
9. D. Bulajic, M. Corsi, G. Cristoforetti, S. Legnaioli, V. Palleschi, A. Salvetti, and E. Tognoni, "A procedure for correcting self-absorption in calibration free-laser induced breakdown spectroscopy," Spectrochim. Acta B At. Spectrosc. **57**(2), 339–353 (2002).
10. H. Amamou, A. Bois, B. Ferhat, R. Redon, B. Rossetto, and P. Matheron, "Correction of Self-Absorption Spectral Line and Ratios of Transition Probabilities for Homogenous and LTE Plasma," J. Quant. Spectrosc. Radiat. Transf. **75**(6), 747–763 (2002).
11. H. Amamou, A. Bois, B. Ferhat, R. Redon, B. Rossetto, and M. Ripert, "Correction of the Self-Absorption for Reversed Spectral Lines: Application to Two Resonance Lines of Neutral Aluminum," J. Quant. Spectrosc. Radiat. Transf. **77**(4), 365–372 (2003).
12. F. Bredice, F. O. Borges, H. Sobral, M. Villagran-Muniz, H. O. Di Rocco, G. Cristoforetti, S. Legnaioli, V. Palleschi, L. Pardini, A. Salvetti, and E. Tognoni, "Evaluation of Self-Absorption of Manganese Emission Lines in Laser Induced Breakdown Spectroscopy Measurements," Spectrochim. Acta B At. Spectrosc. **61**(12), 1294–1303 (2006).
13. A. M. El Sherbini, Th. M. El Sherbini, H. Hegazy, G. Cristoforetti, S. Legnaioli, V. Palleschi, L. Pardini, A. Salvetti, and E. Tognoni, "Evaluation of self-absorption coefficients of aluminum emission lines in laser-induced breakdown spectroscopy measurements," Spectrochim. Acta B At. Spectrosc. **60**(12), 1573–1579 (2005).

Optics EXPRESS

14. I. B. Gornushkin, C. L. Stevenson, B. W. Smith, N. Omenetto, and J. D. Winefordner, "Modeling an inhomogeneous optically thick laser induced plasma: a simplified theoretical approach," Spectrochim. Acta B At. Spectrosc. **56**(9), 1769–1785 (2001).
15. L. Sun and H. Yu, "Correction of self-absorption effect in calibration-free laser-induced breakdown spectroscopy by an internal reference method," Talanta **79**(2), 388–395 (2009).
16. J. M. Li, L. B. Guo, C. M. Li, N. Zhao, X. Y. Yang, Z. Q. Hao, X. Y. Li, X. Y. Zeng, and Y. F. Lu, "Self-absorption reduction in laser-induced breakdown spectroscopy using laser-stimulated absorption," Opt. Lett. **40**(22), 5224–5226 (2015).
17. Y. Tang, J. Li, Z. Hao, S. Tang, Z. Zhu, L. Guo, X. Li, X. Zeng, J. Duan, and Y. Lu, "Multielemental self-absorption reduction in laser-induced breakdown spectroscopy by using microwave-assisted excitation," Opt. Express **26**(9), 12121–12130 (2018).
18. J. J. Hou, L. Zhang, W. B. Yin, Y. Zhao, W. G. Ma, L. Dong, G. Y. Yang, L. T. Xiao, and S. T. Jia, "Investigation on spatial distribution of optically thin condition in laser-induced aluminum plasma and its relationship with temporal evolution of plasma characteristics," J. Anal. At. Spectrom. **32**(8), 1519–1526 (2017).
19. J. Hou, L. Zhang, W. Yin, S. Yao, Y. Zhao, W. Ma, L. Dong, L. Xiao, and S. Jia, "Development and performance evaluation of self-absorption-free laser-induced breakdown spectroscopy for directly capturing optically thin spectral line and realizing accurate chemical composition measurements," Opt. Express **25**(19), 23024–23034 (2017).
20. L. St-Onge, E. Kwong, M. Sabsabi, and E. B. Vadas, "Rapid analysis of liquid formulations containing sodium chloride using laser-induced breakdown spectroscopy," J. Pharm. Biomed. Anal. **36**(2), 277–284 (2004).
21. Q. L. Ma, V. Motto-Ros, X. S. Bai, and J. Yu, "Experimental investigation of the structure and the dynamics of nanosecond laser-induced plasma in 1-atm argon ambient gas," Appl. Phys. Lett. **103**(20), 204101 (2013).
22. X. S. Bai, Q. L. Ma, M. Perrier, V. Motto-Ros, D. Sabourdy, L. Nguyen, A. Jalocha, and J. Yu, "Experimental study of laser-induced plasma: influence of laser fluence and pulse duration," Spectrochim. Acta B At. Spectrosc. **87**(9), 27–35 (2013).
23. V. K. Unnikrishnan, K. Alti, V. B. Kartha, C. Santhosh, G. P. Gupta, and B. M. Suri, "Measurements of plasma temperature and electron density in laser-induced copper plasma by time-resolved spectroscopy of neutral atom and ion emissions," Pramana- J. Phys. **74**(6), 983–993 (2010).